Stable electronic structures of a defective uranofullerene

ARTICLE *in* CARBON · JUNE 2014

Impact Factor: 6.2 · DOI: 10.1016/j.carbon.2014.06.027

CARBON 78 (2014) 19–25

Available at www.sciencedirect.com

ScienceDirect

journal homepage: www.elsevier.com/locate/carbon

Stable electronic structures of a defective uranofullerene

Xing Dai [a], Minsi Xin [a], Yan Meng [a,b], Jie Han [a], Yang Gao [a], Wei Zhang [c], Mingxing Jin [a], Zhigang Wang [a,d,*], Rui-Qin Zhang [b,d,*]

[a] Institute of Atomic and Molecular Physics, Jilin University, Changchun 130012, China
[b] Department of Physics and Materials Science and Centre for Functional Photonics (CFP), City University of Hong Kong, Hong Kong Special Administrative Region, China
[c] Shanghai Institute of Applied Physics, Chinese Academy of Sciences, Shanghai 201800, China
[d] Beijing Computational Science Research Center, Beijing 100084, China

ARTICLE INFO

Article history:
Received 1 December 2013
Accepted 16 June 2014
Available online 23 June 2014

ABSTRACT

Electronic structures and related properties of a defective endohedral metallofullerene $U_2@C_{61}$-Def[5, 6] are studied using density functional theory. It is shown that unlike the $U_2@C_{61}$-Def[6, 6] which has a nonet ground state, the $U_2@C_{61}$-Def[5, 6] has a quintet ground spin state with a lower total energy than the $U_2@C_{61}$-Def[6, 6]. This is due to the antiferromagnetic coupling of the net spin electrons of the U_2 unit with the net spin of both the cage and the adatom. Compared with the $U_2@C_{60}$, the [5, 6]-type defect demonstrates almost no change in the energy gap, while the [6, 6]-type defect does show a reduction. The electronic states and energy gaps of the endohedral metallofullerenes can therefore be engineered in a controllable manner by introducing different adatom-type defects.

1. Introduction

Endohedral metallofullerenes (EMFs) are a kind of novel "super-atomic" system formed by encapsulating a metal atom or a cluster containing metal in the inner space of a fullerene [1,2]. EMFs not only have the physical and chemical properties of fullerene, but also exhibit many of the excellent quantum properties of the inner species [3,4]. The inner metal ions or clusters cannot react with outside substances since the "cage" comprised solely of C atoms provides protection; therefore, toxicity, radioactivity, and many other unfavorable characteristics of the inner species can be effectively avoided. More importantly, the significant charge transfer between the cage and inner clusters means that EMFs have a unique electronic structure. Based on these features, the physicochemical behaviors of the complexes usually surpass the initial components of the fullerene cages and inner atoms/clusters [5]. Therefore, EMFs and their derivatives are expected to have extensive prospects of application in biomedical science [6], electronics [7,8], H storage medium [9], nuclear energy [10], and many other fields. Since $La@C_{82}$ was firstly synthesized at the macroscopic scale [11], more and more other types of EMFs have been synthesized experimentally and their special properties have aroused widespread interest among theorists.

EMFs containing actinide elements have become one of the "hot spots" in actinide chemistry research. These elements, such as U, Th, and Pu, play an important role in nuclear science. Due to the fairly low carbon dioxide emission levels of these elements, they show great potential in nuclear energy. The relevant nanomaterials and technology are

* *Corresponding authors:* Fax: +86 431 85168816 (Z. Wang), +852 34420538 (R.-Q. Zhang).
E-mail addresses: wangzg@jlu.edu.cn (Z. Wang), aprqz@cityu.edu.hk (R.-Q. Zhang).
http://dx.doi.org/10.1016/j.carbon.2014.06.027
0008-6223/

considered to have reached a key stage in the development of nuclear power [12]. After Guo et al. synthesized $U@C_{28}$ experimentally in 1991 for the first time [13], its related geometrical structure and electronic properties have been obtained from theoretical studies [14]. Subsequently, Diener and co-worker synthesized $U@C_{74}$ and $U@C_{82}$ [15]. The electronic structure features of $U@C_{82}$ have also been explained through theoretical calculations using density functional theory (DFT) [16]. Although C_{28} and C_{82} fullerenes are usually unstable, they can be stabilized by inserting the U atom into their cages. Besides, it has been successfully used to stabilize non-IPR fullerenes by encapsulating other metal atom/molecule [17]. In fact, strong signals of $U_2@C_{60}$, including many other EMF structures, are also observed in Guo's Fourier transform mass spectrometry experiment, proving that the two U atoms were embedded into fullerene cavities rather than being attached to their surfaces [13]. Theorists have accordingly predicted that fullerene may be able to encapsulate two U atoms based on quantum first principles calculations [18,19] and pointed out that the size effect of the inner space means an unprecedented sixfold one-electron-two-center metal–metal bond is formed between the two U atoms in C_{60} fullerene [18]. However, if we enlarge these to, say, C_{70} and C_{84}, the U–U bond will be completely dissociated and each U atom will tend to bond on the inner wall [19]. Actinide metallofullerenes not only have the thermal stability of the fullerene, but also the physicochemical properties of the actinide. They are likely therefore to have important applications in advanced fuel technology.

Most of the novel properties of EMFs can be attributed to their unique electronic structures. In EMF systems, the internal metal atoms always donate electrons to the fullerene cage and carry considerable positive charge. Previous reports show that electrons on the cage surface transferred from the inner metal atoms will preferentially adopt a stable closed-shell electronic configuration [20]. The remaining electrons on the surface of the outer cage will generally take an antiferromagnetic coupling with the net spin of the inner metal atoms [16,21]. There is no doubt that changes in the electronic structure of EMFs will result in many properties of the whole system also changing. Thus, from a theoretical point of view, exploring possible ways to adjust their electronic structure [22,23], including the number of charges transferred and the coupling mode of the net spin electrons is an interesting and important subject of study. When encapsulating a U_2 molecule into C_{60} fullerene, EMF $U_2@C_{60}$ has a septet ground state resulting from a ferromagnetic coupling of six unpaired electrons on the two U atoms. No net spin electron remains on the fullerene [18]. However, it is well known that defects can easily form in carbon materials such as fullerenes, nanotubes, and graphene. These can bring about a significant change in the electronic structure as well as many other properties [24,25]. Our previous study suggests that a [6, 6] defect (adsorbing a carbon atom on a [6, 6] bond of C_{60} fullerene) could induce a nonet ground spin state for the $U_2@C_{61}$-Def[6, 6] system. This can be attributed to the ferromagnetic coupling between the spin of the unpaired electrons of the two U atoms with the C adatom contributing to this spin state [26].

C_{60} has [6, 6] (connecting two hexagons) and [5, 6] (connecting a pentagon and a hexagon) C–C bonds. This means that only two kinds of adatom-type defects can be formed on its surface. Our previous studies show that the total energy of the $U_2@C_{61}$-Def[6, 6] will reach a minimum when adsorbing a C atom on the [6, 6] C–C bond which lies along the U–U axis near one U atom. In this study, we introduce a C adatom on the [5, 6] C–C bond of the cage surface of the $U_2@C_{60}$ and consider all the possible isomers. More detailed calculations are performed for the most stable $U_2@C_{61}$-Def[5, 6] structure, and we also present a comparative analysis of the properties of $U_2@C_{60}$, $U_2@C_{61}$-Def[6, 6] and $U_2@C_{61}$-Def[5, 6] systems. Our results show that $U_2@C_{61}$-Def[5, 6] is more stable than $U_2@C_{61}$-Def[6, 6]. The impact of the [5, 6] defect is different to the [6, 6], particularly in terms of the electronic structure. The [5, 6] defect results in a new and interesting coupling mechanism for the net spin electrons in the $U_2@C_{61}$-Def[5, 6] system.

2. Theoretical calculations

Relativistic effects and electron correlation must be taken into consideration when dealing with actinide-containing systems. In this paper we use a relativistic pseudopotential method to take into account relativistic effects. A (14s13p10d8f6g)/[10s9p5d4f3g] valance basis set with corresponding quasi-relativistic small-core pseudopotential with 60 core-electrons treatment [27] was chosen for U atoms. A double-split basis set, 3-21G [28], was chosen for C atoms. The advantages of this choice of basis sets are discussed in previous reports [26,29,30]. A significant advantage of DFT calculations is the ability to account for the electron correlation [31]. As such, BP86 [32] and PBE [33] exchange correlation (XC) functionals have been particularly widely used in the calculation of actinide EMFs [18,19,26]. Therefore, both XC-functionals are employed for all geometrical optimization calculations in this work. Frequency calculations are performed at the same theoretical level in order to ensure the structures obtained are real minima on the potential energy surface. Satisfyingly, the two methods produce consistent predictions for the geometry and electronic structures of all systems we considered. The further property results we present here are therefore based on the calculations using the BP86 functional. For all the relevant systems, spin polarization DFT methods are used for all calculations under a variety of multiplicities. All calculations are performed using the Gaussian 09 program [34].

3. Results and discussion

3.1. *Geometric structures of $U_2@C_{61}$-Def[5, 6], $U_2@C_{60}$, and $U_2@C_{61}$-Def[6, 6]*

We introduce a [5, 6]-type defect into the initial $U_2@C_{60}$ system. According to the different adsorbing sites of the adatom, $U_2@C_{61}$-Def[5, 6] has six isomers which are defined as structures (a)–(f) in Fig. 1. Full geometrical optimization calculations are performed for each isomer at different multiplicities using the BP86 method. The stable structures, ground electronic states, and total energy relationship are

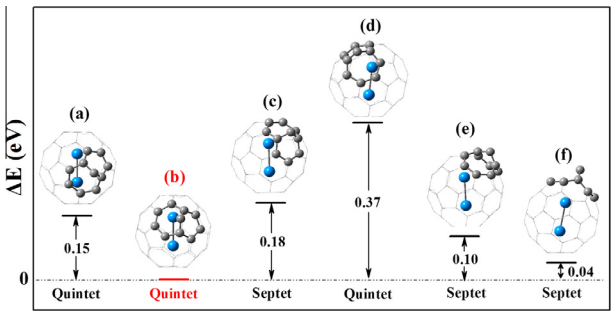

Fig. 1 – The stable structures, ground states, and total energy relationship for the six isomers of $U_2@C_{61}$-Def[5, 6]. (A color version of this figure can be viewed online.)

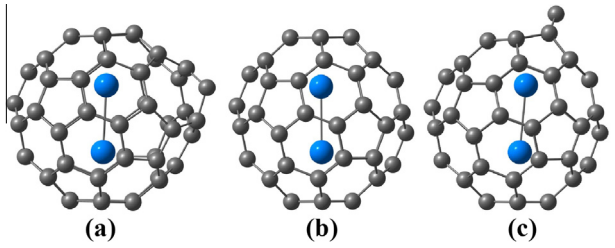

Fig. 2 – (a)–(c) Represent the equilibrium geometry structures of $U_2@C_{61}$-Def[5, 6], $U_2@C_{60}$, and $U_2@C_{61}$-Def[6, 6], respectively. (A color version of this figure can be viewed online.)

summarized in Fig. 1. More detailed total energy data for each isomer can be seen in the Supporting information.

From Fig. 1, it can be seen that structure (b) of the $U_2@C_{61}$-Def[5, 6] has the lowest total energy of the six isomers. Therefore, we focus on this structure and discuss its properties in the following section. The most stable $U_2@C_{61}$-Def[5, 6] structure (structure (b) in Fig. 1) can be characterized as the adatom adsorbing on a [5, 6] C–C bond near the equatorial area of the initial $U_2@C_{60}$ surface, as also shown in Fig. 2(a). Based on calculations at the same theoretical level, the stable $U_2@C_{60}$ and $U_2@C_{61}$-Def[6, 6] structures which have been already reported [18,26] are obtained again, as depicted in Fig. 2(b) and (c), respectively. In the $U_2@C_{60}$, the U_2 unit is sandwiched between two six-membered rings. In contrast to the $U_2@C_{61}$-Def[5, 6] (Fig. 2(a)), the adatom favors adsorption on a [6, 6] C–C bond of a hexagon, faced by one U atom and forming the stable $U_2@C_{61}$-Def[6, 6] (Fig. 2(c)). Therefore, there are significant differences in the adatom positions when forming [5, 6] and [6, 6] defects on the $U_2@C_{60}$ surface. The relevant calculations for the three fullerenes of C_{60}, C_{61}-Def[5, 6] and C_{61}-Def[6, 6] are also performed and discussed in the Supporting information.

Previous studies suggest that the U–U distance would be elongated compared to the isolated U_2 molecule when encapsulating into C_{60} fullerene, due to the rejection between the two U cations and the mixture of ionic and covalent interaction between the U atoms and the inner wall [18]. If the cavity is large enough, the U_2 molecule will dissociate completely [19]. Both types of defects could enlarge the local size of the fullerene, so the $U_2@C_{61}$-Def[5, 6] and the $U_2@C_{61}$-Def[6, 6] have a longer U–U distance than that of the $U_2@C_{60}$. Our calculated bond length of the isolate U_2 molecule is 2.27 Å (see Supporting information for details), consistent with previous DFT results [19]. According to Wu [18], the U–U distance in $U_2@C_{60}$ is 2.72 Å, and ours is about 2.71 Å (see Supporting information) which is very close. Due to the size effect, the U_2 unit has a longer U–U distance (about 2.81 Å) in the $U_2@C_{61}$-Def[6, 6], exactly as shown in our previous report [26]; the distance between U atoms is about 2.76 Å in the $U_2@C_{61}$-Def[5, 6] system which is larger than the $U_2@C_{60}$ case but shorter than the $U_2@C_{61}$-Def[6, 6] case (see Table 1).

Table 1 shows the relative energy of the two defective EMFs with different multiplicities. The $U_2@C_{61}$-Def[6, 6] and $U_2@C_{61}$-Def[5, 6] are essentially isomers, but the latter has a lower total energy (see Table 1). We further calculated the spin–orbit effects on the electron structure, all the results revealed that $U_2@C_{61}$-def[5, 6] has a quintet ground state (see Supporting information Part 3). This indicates that the [5, 6]-type adatom defect may be more easily formed on the surface of the $U_2@C_{60}$. In addition, the energy gap between the Highest Occupied Molecular Orbital (HOMO) and the Lowest Unoccupied Molecular Orbital (LUMO) of the two isomers are summarized in Table 1. We obtain a gap value of $U_2@C_{60}$ of about 0.12 eV (see Supporting information). The $U_2@C_{61}$-Def[6, 6] system has a gap value of about 0.05 eV (see Table 1) which is obviously smaller. The gap value for

Table 1 – Electronic states and relative energies of the $U_2@C_{61}$-Def[5, 6] and $U_2@C_{61}$-Def[6, 6].

Method	Systems	Multiplicity	ΔE (eV)	Gap (eV)	R_{U-U} (Å)
BP86	[5, 6]	Triplet	0.07		
		Quintet	0	0.11	2.76
		Septet	0.01		
	[6, 6]	Septet	0.30		
		Nonet	0.28	0.05	2.81
		11-et	0.82		
PBE	[5, 6]	Triplet	0.14		
		Quintet	0	0.11	2.77
		Septet	0.01		
	[6, 6]	Septet	0.30		
		Nonet	0.29	0.06	2.82
		11-et	0.84		

the $U_2@C_{61}$-Def[5, 6] is about 0.11 eV (see Table 1) which is similar to the $U_2@C_{60}$. In fact, we also find an $U_2@C_{61}$-Def[5, 6] structure which has an obviously higher HOMO–LUMO gap than $U_2@C_{60}$. For the ground state of isomer (f) (see Fig. 1), the gap value is about 0.21 eV; however, this structure has a slightly higher total energy than the isomer (b). Therefore, introducing different adatom-type defects for the $U_2@C_{60}$ system could be a controllable way to adjust the HOMO–LUMO gap. This method is expected to provide a reference point for the control technique in molecular electronics.

3.2. *Electronic structures of the three ground-state EMFs*

The $U_2@C_{60}$ has a septet ground state (see Supporting information) while the $U_2@C_{61}$-Def[6, 6] has a nonet ground state which is affected by the [6, 6]-type defect (see Table 1), consistent with previous studies [18,26]. Interestingly, induced by the [5, 6]-type defect, the $U_2@C_{61}$-Def[5, 6] system has a quintet ground spin state with a unique cause of formation, as seen from the analysis of its electronic structures. In this section, we will explain the features of the electronic structure of the $U_2@C_{61}$-Def[5, 6], compared with that of the $U_2@C_{60}$ and the $U_2@C_{61}$-Def[6, 6].

The electronic structures of EMFs depend on the number of intramolecular charge transfer and the coupling mode of unpaired electrons between the cage and the inner metal. In general, the internal metal atoms always donate electrons to the fullerene cage. Electrons on the surface of the cage preferentially adopt a stable closed-shell electronic configuration [20]. If electrons remain on the surface, they often tend to form an antiferromagnetic coupling with the net spin electrons of the metal atoms. This phenomenon occurs in many EMFs such as $U@C_{82}$, $Gd@C_{82}$, and so on [16,21].

Fig. 3(a) shows the spin density distribution of the ground state $U_2@C_{61}$-Def[5, 6]. Based on calculations at the same theoretical level, we also obtain that of the $U_2@C_{60}$ and $U_2@C_{61}$-Def[6, 6] as depicted in Fig. 3(b) and (c), respectively, which agree with previous reports [18,26]. We can clearly understand the sources of net spin electrons and their coupling modes. In the $U_2@C_{61}$-Def[5, 6], there are considerable net spin-up electrons on the two U atoms (about 5.8; see Table 2), and about 0.9 net spin-down electrons on the adatom, the same amount as found on the surface of the cage. In this way, the total number for the net spin of

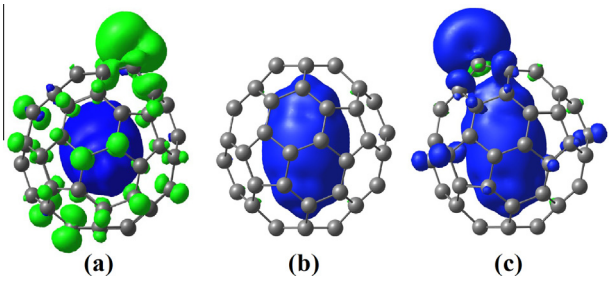

Fig. 3 – (a)–(c) Present the spin density of the ground state of $U_2@C_{61}$-Def[5, 6], $U_2@C_{60}$, and $U_2@C_{61}$-Def[6, 6], respectively. The blue areas correspond to the spin-up electrons, and the green areas to the spin-down electrons. (Isovalue = 0.002 a. u.). (A color version of this figure can be viewed online.)

the whole system equals four and thus the quintet ground state is formed. In fact, there are three important characters of the coupling mode among these net spin electrons in the $U_2@C_{61}$-Def[5, 6]. Firstly, the unpaired electrons on the two U atoms are coupled in a ferromagnetic mode, similar to the case of the isolate U_2 molecule [35] and retaining the character of the $U_2@C_{60}$ (see Fig. 3(b)) at the same time. Secondly, the unpaired electrons between the cage and the inner metal atoms are coupled in an antiferromagnetic mode, as seen in many EMFs [16,21]. Thirdly, unlike the $U_2@C_{61}$-Def[6, 6] in which the adatom's net spins take a ferromagnetic coupling with that of the inner metal atoms (see Fig. 3(c)), in the $U_2@C_{61}$-Def[5, 6] the net spin electrons between the adatom and the inner metal atoms are coupled in an antiferromagnetic mode (see Fig. 3(a)). Based on this discussion, it can be seen that three kinds of effect contribute to this complex coupling mode induced by the [5, 6]-type defect and forming a unique quintet ground state in the $U_2@C_{61}$-Def[5, 6]. This indicates that the magnetic properties of EMFs could be controlled by introducing different type of adatom defects on the cage surface.

We note that the contribution of the net spin electrons on the adatom is almost provided by the 2p shell of the C atom in $U_2@C_{61}$-Def[5, 6] (Fig. 3(a)); however, in the $U_2@C_{61}$-Def[6, 6], the net spin on the adatom results from a hybridization of 2s and 2p shells of C atom (Fig. 3(c)). For this reason, the adatom has some less unpaired electrons of the adatom in the

Table 2 – Population analysis of net spin and Mulliken charge. C^{61th} is the adatom, U^{1st} and U^{2nd} are the U atoms near and far from the defect, respectively. These two U atoms are equivalent in the $U_2@C_{60}$. For the number of net spin electrons, the negative sign indicates spin down and the positive one spin up.

Method	Systems	Net Spin			Mulliken Charge		
		C^{61th}	U^{1st}	U^{2nd}	C^{61th}	U^{1st}	U^{2nd}
BP86	[5, 6]	−0.9	3.0	2.8	0.10	2.35	2.34
	$U_2@C_{60}$		3.1	3.1		2.33	2.33
	[6, 6]	1.5	3.0	3.3	0.07	2.48	2.36
PBE	[5, 6]	−1.0	3.0	2.8	0.10	2.32	2.30
	$U_2@C_{60}$		3.1	3.1		2.29	2.29
	[6, 6]	1.5	3.0	3.3	0.09	2.50	2.32

$U_2@C_{61}$-Def[5, 6] (about 0.9, spin down, see Table 2) than that in $U_2@C_{61}$-Def[6, 6] (about 1.5, spin up), resulting in the spin-down electrons occurring on the cage surface.

3.3. Charge distribution

In the $U_2@C_{60}$, the internal metal atoms take significant positive charges and present cationic states caused by their electron donation to the fullerene. Therefore, there is a strong electrostatic attraction between the metal atoms and the inner wall, similar to the ionic interactions. At the same time, if the U_2 molecule is encapsulated in fullerenes, the repulsive interaction between the two cations becomes more obvious. Both the metal-cage electrostatic attraction and the metal–metal repulsive interaction result in an increase in the U–U distance in the $U_2@C_{60}$ compared to the isolated U_2 molecule [18].

The charge distributions of the three atoms we focus on here are summarized in Table 2. It can be seen that each U atom donates about 2.33 electrons to the C_{60} fullerene in the $U_2@C_{60}$. Most of the negative charge in the cage is gathered at the two polar areas of the $U_2@C_{60}$ and symmetrically distributed. A small number of negative charges are distributed on the equatorial region. Once the two types of defect are introduced, obvious changes take place in the charge distribution of the two U atoms. In contrast to the $U_2@C_{60}$, the two U atoms take a slightly more positive charge in the $U_2@C_{61}$-Def[5, 6], while the two U atoms take a significantly more positive charge in the $U_2@C_{61}$-Def[6, 6], especially the U^{1st} atom because it is closer to the defect than the U^{2nd} and hence the impact is stronger. Therefore, the [6, 6]-type defect conduces the U^{1st} atom to take more positive charge than the U^{2nd}. In the $U_2@C_{61}$-Def[6, 6], the adatom takes a small amount of positive charge. So, the two C atoms which are bonded to the adatom in the $U_2@C_{61}$-Def[6, 6] represent, comparatively speaking, the maximum of the negative charge among all the C atoms, as they have gained electrons from both the inner U atom and the outer C adatom. However, in the $U_2@C_{61}$-Def[5, 6], most of the negative charge on the cage remains distributed around the poles because the defect is further from the U atoms. More details of the charge distribution on the two C atoms near the adatom can be found in the Supporting information.

Based on the above discussion we conclude that if the defect is near one inner U atom, more charge transfer from it to the cage can be induced, such as is seen in the $U_2@C_{61}$-Def[6, 6]. On the contrary, if the defect is far from the two inner U atoms, their charge transfer will be almost unaffected compared to the initial $U_2@C_{60}$ case, such as is seen in the $U_2@C_{61}$-Def[5, 6].

3.4. Interactions of the U–U and U-cage

Based on the eigenstates of the DFT calculations, we also obtain and analyze the electron densities of the different systems in order to understand the U–U and U-cage interactions qualitatively. Fig. 4 displays the electron densities of three EMFs in a plane containing the two U atoms. It can be seen that there are significant electron accumulations (green areas) between the neighboring C atoms forming a C–C covalent bond. By contrast, no significant accumulation appears between those C atoms located in the para-position of a hexagon or the meta-position of a pentagon.

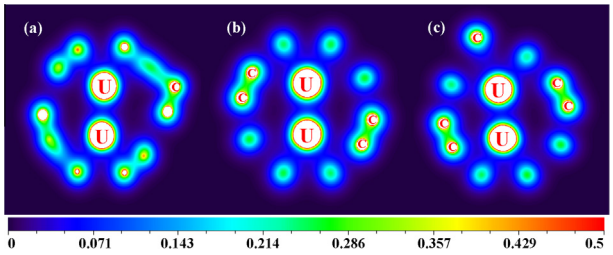

Fig. 4 – (a)–(c) Represent the electron density color-filled maps of the $U_2@C_{61}$-Def[5, 6], $U_2@C_{60}$, and $U_2@C_{61}$-Def[6, 6], respectively. (A color version of this figure can be viewed online.)

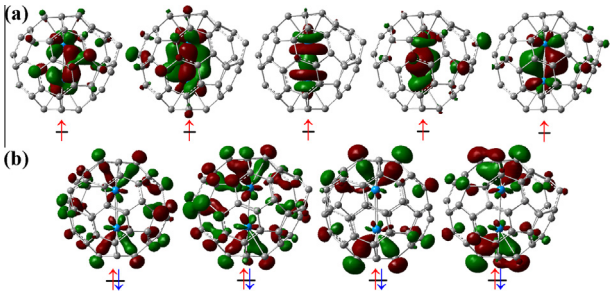

Fig. 5 – (a) Five single electron-occupied molecular orbitals of the $U_2@C_{61}$-Def[5, 6] revealing covalent interactions between the two U atoms; and (b) four double electron-occupied molecular orbitals of the $U_2@C_{61}$-Def[5, 6] with a much lower energy, revealing covalent interactions between the U atoms and the cage. (Isovalue = 0.035 a. u.). (A color version of this figure can be viewed online.)

From Fig. 4, there are significant electron accumulations between two internal U atoms for all the three cases, indicating that a covalent interaction exists between them. Meanwhile, Fig. 5(a) depicts the relevant frontier molecular orbitals which provide the U–U covalent character in the $U_2@C_{61}$-Def[5, 6]. These five molecular orbitals are all mainly dominated by the 5f orbitals of the U atoms. Because of the impact of the defect, they undergo some deformations. Integrating all this information indicates that the U_2 molecule cannot be dissociated when it is encapsulated into these particular three fullerenes. In addition, we also observe electron accumulations between each U atom and the inner wall. For the $U_2@C_{61}$-Def[5, 6] on which we have focused in this paper, a more careful inspection of the molecular orbitals reveals substantial covalent interactions between the U atoms and the cage, as depicted in Fig. 5(b). These orbitals can be described as hybridizations between the π orbitals of the cage and the 5f orbitals of the U atoms. Therefore, the U atom and the cage interact through a mixture of ionic and covalent bonds, similar to the $U_2@C_{60}$ case [18].

We also obtained the molecular orbital information for the $U_2@C_{60}$ and $U_2@C_{61}$-Def[6, 6] based on calculations at the same theoretical level. These are presented in the Supporting information. For the $U_2@C_{60}$, we predicted the sixfold single

electron U–U covalent bond by observing the six single electron-occupied orbitals which is fully consistent with the results found by Wu. By comparison, fewer than six orbitals reflect the U–U covalent bond across the two defective EMFs. These results indicate that, to a certain extent, the adatom defects destroy the inner U–U covalent bond and increase the U–U distance relative to the $U_2@C_{60}$.

4. Conclusions

We have calculated the electronic structures and related properties of a defective EMF $U_2@C_{61}$-Def[5, 6], and undertaken a comprehensive comparison with the results of $U_2@C_{60}$ and the $U_2@C_{61}$-Def[6, 6]. Our results show that the $U_2@C_{61}$-Def[5, 6] is more stable than the $U_2@C_{61}$-Def[6, 6]. The [5, 6]-type defect induces a complex and interesting electronic structure for the $U_2@C_{61}$-Def[5, 6] system. In the ground state of the $U_2@C_{61}$-Def[5, 6], the net spin electrons between the two U atoms are coupled in a ferromagnetic mode; however, the net spin electrons of the cage and the adatom take an antiferromagnetic coupling mode with the inner U atoms. This special coupling mechanism is quite different from that of the $U_2@C_{61}$-Def[6, 6], and gives the $U_2@C_{61}$-Def[5, 6] system a unique quintet ground spin state. The $U_2@C_{61}$-Def[5, 6] has a similar HOMO–LUMO gap to that of the $U_2@C_{60}$ (about 0.11 eV), while the $U_2@C_{61}$-Def[6, 6] has a smaller gap value (about 0.05 eV). The charge analysis shows that compared to the $U_2@C_{60}$, the [5, 6]-type defect results in almost no change to the charge distribution on the U atoms, but the U_2 unit will donate more electrons to the cage by introducing the [6, 6]-type defect. In addition, in the three different cavities, both the electron density and molecular orbitals analysis indicate that the U–U and U-cage interactions are covalent in nature. Although the U–U distances are elongated relative to the isolate U_2 molecule in the three fullerenes, the U_2 unit cannot be completely dissociated. The U atom and the cage interact through a mixture of ionic and covalent bonds.

Based on the foregoing, the two defective EMFs of the $U_2@C_{61}$-Def[5, 6] and the $U_2@C_{61}$-Def[6, 6] systems could be given even richer and more diverse electronic state structures by introducing one adatom-type defect on the different surface site of the initial $U_2@C_{60}$. Our results provide an optional approach for adjusting the electronic state and the HOMO–LUMO gap of the EMFs in a controllable manner. By discussing the different impact on the properties of the initial $U_2@C_{60}$ when introducing different spin polarization defects, we have reached a deeper understanding of the complex interaction between the internal metal atom and the outer cage of EMFs. This study is expected to promote the development of new actinide materials and novel molecular materials for use in spintronics and electronics.

Acknowledgments

We wish to thank the Strategically Leading Program of the Chinese Academy of Sciences (Grant No. XDA02040100) and the support of the National Science Foundation of China under Grant Nos. 11374004 and 11004076. Z. W. also acknowledges the assistance of the Fok Ying Tung Education Foundation (142001) and the High Performance Computing Center (HPCC) of Jilin University.

Appendix A. Supplementary data

Supplementary data associated with this article can be found, in the online version, at http://dx.doi.org/10.1016/j.carbon.2014.06.027.

REFERENCES

[1] Shinohara H. Endohedral metallofullerenes. Rep Prog Phys 2000;63(6):843–92.
[2] Popov AA, Yang S, Dunsch L. Endohedral metallofullerenes. Chem Rev 2013;113(8):5989–6113.
[3] Stevenson S, Rice G, Glass T, Harich K, Cromer F, Jordan MR, et al. Small-bandgap endohedral metallofullerenes in high yield and purity. Nature 1999;401(6748):55–7.
[4] Wang CR, Kai T, Tomiyama T, Yoshida T, Kobayashi Y, Nishibori E, et al. A scandium carbide endohedral metallofullerene: $(Sc_2C_2)@C_{84}$. Angew Chem Int Ed 2001;40(2):397–9.
[5] Yamada M, Akasaka T, Nagase S. Endohedral metal atoms in pristine and functionalized fullerene cages. Acc Chem Res 2010;43(1):92–102.
[6] Kang SG, Zhou G, Yang P, Liu Y, Sun B, Huynh T, et al. Molecular mechanism of pancreatic tumor metastasis inhibition by $Gd@C_{82}(OH)_{22}$ and its implication for de novo design of nanomedicine. Proc Natl Acad Sci USA 2012;109(38):15431–6.
[7] Wang T, Wu J, Xu W, Xiang J, Lu X, Li B, et al. Spin divergence induced by exohedral modification: ESR study of $Sc_3C_2@C_{80}$ fulleropyrrolidine. Angew Chem Int Ed 2010;49(10):1786–9.
[8] Yang SF, Fan L, Yang S. Significantly enhanced photocurrent efficiency of a poly(3-hexylthiophene) photoelectrochemical device by doping with the endohedral metallofullerene $Dy@C_{82}$. Chem Phys Lett 2004;388(4–6):253–8.
[9] Fujii A, Umeda T, Shirakawa T. Photocurrent enhancement in conducting polymer device by doping with endohedral metallofullerene $La@C_{82}$. Jpn J Appl Phys 2002;41:2254–5.
[10] Shi W, Zhao Y, Chai Z. A preview of Nano-materials and nano-technologies applied in advanced nuclear energy system. Prog Chem 2011;23(7):1478–84.
[11] Chai Y, Guo T, Jin C, Haufler RE, Chibante LF, Fure J, et al. Fullerenes with metals inside. J Phys Chem 1991;95(20):7564–8.
[12] Hill DJ. Nuclear energy for the future. Nat Mater 2008;7(9):680–2.
[13] Guo T, Diener MD, Chai Y, Alford MJ, Haufler RE, McClure SM, et al. Uranium stabilization of C_{28}: a tetravalent fullerene. Science 1992;257(5077):1661–4.
[14] Zhao K, Pitzer RM. Electronic structure of C_{28}, $Pa@C_{28}$, and $U@C_{28}$. J Phys Chem 1996;100(12):4798–802.
[15] Akiyama K, Zhao Y, Sueki K, Tsukada K, Haba H, Nagame Y, et al. Isolation and characterization of light actinide metallofullerenes. J Am Chem Soc 2001;123(1):181–2.
[16] Liu X, Li L, Liu B, Wang D, Zhao Y, Gao X. Theoretical study on the ground state structure of uranofullerene $U@C_{82}$. J Phys Chem A 2012;116(47):11651–5.
[17] Yang T, Zhao X, Nagase S. Quantum chemical insight of the dimetallic sulfide endohedral fullerene $Sc_2S@C_{70}$: does it possess the conventional D_{5h} cage? Chem Eur J 2013;19(8):2649–54.

[18] Wu X, Lu X. Dimetalloendofullerene $U_2@C_{60}$ has a U–U multiple bond consisting of sixfold one-electron-two-center bonds. J Am Chem Soc 2007;129(7):2171–7.
[19] Infante I, Gagliardi L, Scuseria GE. Is fullerene C_{60} large enough to host a multiply bonded dimetal? J Am Chem Soc 2008;130(23):7459–65.
[20] Fan MF, Lin Z, Yang S. Closed-shell electronic requirements for small fullerene cage structures. J Mol Struct (THEOCHEM) 1995;337(3):231–40.
[21] Sebetci A, Richter M. $Gd@C_{82}$: origin of the antiferromagnetic coupling between endohedral Gd and the free spin on the carbon cage. J Phys Chem C 2000;114(1):15–9.
[22] Xu J, Li M, Shi Z, Gu Z. Electrochemical survey: the effect of the cage size and structure on the electronic structures of a series of ytterbium metallofullerenes. Chem Eur J 2005;12(2):562–7.
[23] Chamberlain TW, Champness NR, Schroder M, Khlobystov AN. A piggyback ride for transition metals: encapsulation of exohedral metallofullerenes in carbon nanotubes. Chem Eur J 2011;17(2):668–74.
[24] Xin MS, Wang FT, Meng Y, Tian CJ, Jin MX, Wang ZG, et al. Characteristic vibrational modes and electronic structures of carbon nanotubes containing defects. J Phys Chem C 2012;116(1):292–7.
[25] Lehtinen PO, Foster AS, Ayuela A, Vehvilainen TT, Nieminen RM. Structure and magnetic properties of adatoms on carbon nanotubes. Phys Rev B 2004;69(15):155422.
[26] Dai X, Cheng C, Zhang W, Xin MS, Huai P, Zhang RQ, et al. Defect induced electronic structure of uranofullerene. Sci Rep 2013;3:1341.
[27] Cao X, Dolg M. Segmented contraction scheme for small-core actinide pseudopotential basis sets. J Mol Struct (THEOCHEM) 2004;673(1–3):203–9.
[28] Binkley JS, Pople JA, Hehre J. Self-consistent molecular orbital methods. 21. Small split-valence basis sets for first-row elements. J Am Chem Soc 1980;102(3):939–47.
[29] Cong Y, Yang ZZ, Wang CS, Liu XC, Bao XH. Investigation of the regio- and stereoselectivity of Diels-Alder reactions by newly developed ABEEM σπ model on the basis of local HSAB principle and maximum hardness principle. Chem Phys Lett 2002;357(1–2):59–64.
[30] Xin MS, Dai X, Huang BL, Meng Y, Feng W, Jin MX, et al. Basis set effect on defect induced spin polarization of a carbon nanotube in density functional theory calculations. Chem Phys Lett 2013;585:107–11.
[31] Kutepov AL. The effect of exact calculation of exchange interaction upon calculated electronic structure of actinides. J Alloy Compd 2007;444–445:174–6.
[32] Perdew JP. Density-functional approximation for the correlation energy of the inhomogeneous electron gas. Phys Rev B 1986;33(12):8822–4.
[33] Perdew JP, Burke K, Ernzerhof M. Generalized gradient approximation made simple. Phys Rev Lett 1996;77(18):3865–8.
[34] Frisch MJ, Trucks GW, Schlegel HB, Scuseria GE, Robb MA, JR, et al. Gaussian 09, Revision D.01. Wallingford, CT: Gaussian Inc; 2013.
[35] Gagliardi L, Roos B. Quantum chemical calculations show that the uranium molecule U_2 has a quintuple bond. Nature 2005;433(7028):848–51.